Germanium photodetector with 60 GHz bandwidth using inductive gain peaking

Ari Novack,[1,2,*] Mike Gould,[3] Yisu Yang[4], Zhe Xuan[4], Matthew Streshinsky,[1,2] Yang Liu[4], Giovanni Capellini,[5] Andy Eu-Jin Lim,[1] Guo-Qiang Lo,[1] Tom Baehr-Jones,[3] and Michael Hochberg[1,2,3]

[1]*Institute of Microelectronics, A*STAR (Agency for Science, Technology and Research), 11 Science Park Road, Singapore Science Park II, 117685, Singapore*
[2]*Department of Electrical and Computer Engineering, National University of Singapore, 4 Engineering Drive 3, Singapore 117576, Singapore*
[3]*Department of Electrical Engineering, University of Washington, Seattle, Washington 98195, USA*
[4]*Department of Electrical and Computer Engineering, University of Delaware, Newark, Delaware 19716, USA*
[5]*Dipartimento di Scienze, Università degli Studi Roma Tre, Rome, 00146, Italy*
[*]*arinovack@nus.edu.sg*

Abstract: Germanium-on-silicon photodetectors have been heavily investigated in recent years as a key component of CMOS-compatible integrated photonics platforms. It has previously been shown that detector bandwidths could theoretically be greatly increased with the incorporation of a carefully chosen inductor and capacitor in the photodetector circuit. Here, we show the experimental results of such a circuit that doubles the detector 3dB bandwidth to 60 GHz. These results suggest that gain peaking is a generally applicable tool for increasing detector bandwidth in practical photonics systems without requiring the difficult process of lowering detector capacitance.

OCIS codes: (040.6070) Solid state detectors; (060.5625) Radio frequency photonics; (130.0130) Integrated optics; (250.0250) Optoelectronics.

References and links

1. R. Soref, "The past, present, and future of silicon photonics," IEEE J. of Sel. Top. in Quantum Electronics **12**(6), 1678–1687 (2006).
2. M. Hochberg and T. Baehr-Jones, "Towards fabless silicon photonics," Nature Photonics **4**(8), 492–494 (2010).
3. L. Colace, G. Masini, F. Galluzzi, G. Assanto, G. Capellini, L. Di Gaspare, E. Palange, and F. Evangelisti, "Metal–semiconductor–metal near-infrared light detector based on epitaxial Ge/Si," Appl. Phys. Letters **72**(24), 3175-3177 (1998).
4. L. Colace, G. Masini, G. Assanto, H.-C. Luan, K. Wada, and L. C. Kimerling, "Efficient high-speed near-infrared Ge photodetectors integrated on Si substrates," Appl. Phys. Letters **76**(10), 1231-1233 (2000).
5. J. Michel, J. Liu, L. C. Kimerling, "High-performance Ge-on-Si photodetectors," Nature Photonics **4**, 527–534 (2010).
6. L. Vivien, J. Osmond, J.-M. Fédéli, D. Marris-Morini, P. Crozat, J.-F. Damlencourt, E. Cassan, Y. Lecunff, and S. Laval, "42 GHz p.i.n Germanium photodetector integrated in a silicon-on-insulator waveguide," Optics Express **17**(8), 6252–6257 (2009).
7. S. Liao, N.-N. Feng, D. Feng, P. Dong, R. Shafiiha, C.-C. Kung, H. Liang, W. Qian, Y. Liu, J. Fong, J. E. Cunningham, Y. Luo, and M. Asghari, "36 GHz submicron silicon waveguide germanium photodetector," Optics Express **19**(11), 10967–10972 (2011).
8. C. T. DeRose, D. C. Trotter, W. A. Zortman, A. L. Starbuck, M. Fisher, M. R. Watts, and P. S. Davids, "Ultra compact 45 GHz CMOS compatible Germanium waveguide photodiode with low dark current," Optics Express **19**(25) 24897–24904 (2011).
9. L. Vivien, A. Polzer, D. Marris-Morini, J. Osmond, J. M. Hartmann, P. Crozat, E. Cassan, C. Kopp, H. Zimmermann, and J. M. Fédéli, "Zero-bias 40Gbit/s germanium waveguide photodetector on silicon," Optics Express **20**(2) 1096–1101 (2012).
10. S. Shekhar, J. Walling, and D. Allstot, "Bandwidth Extension Techniques for CMOS Amplifiers," IEEE Journal of Solid-State Circuits **41**(11) 2424–2439, (2006).

11. C. Wu, C. Lee, W. Chen, and S. Liu, "CMOS wideband amplifiers using multiple inductive-series peaking technique," IEEE Journal of Solid-State Circuits **40**(2), 548–552 (2005).
12. J. Morikuni and S. Kang, "An analysis of inductive peaking in photoreceiver design," Journal of Lightwave Technology **10**(10), 1426-1437 (1992).
13. S. Mohan, M. Hershenson, S. Boyd, and T. Lee, "Bandwidth extension in CMOS with optimized on-chip inductors," IEEE Journal of Solid-State Circuits **35**(3), 346–355 (2000).
14. J. Morikuni and S. Kang, "An analysis of inductive peaking in high-frequency amplifiers," in *Proceedings of IEEE International Symposium on Circuits and Systems*, (San Diego, Calif., 1992), pp. 2848–2851.
15. J. Orcutt and R. Ram, "Photonic device layout within the foundry CMOS design environment," Photonics Technology Letters, IEEE **22**(8), 544–546 (2010).
16. G. Rangel-Sharp, R. E. Miles, S. Iezekiel, "Physical Modeling of Traveling-Wave Heterojunction Phototransistors," Journal of Lightwave Technology **26**(13), 1943–1949 (2008).
17. M. Piels, A. Ramaswamy, and J. E. Bowers, "Nonlinear modeling of waveguide photodetectors," Optics Express **21**(13), 15634–15644 (2013).
18. J. Wang and S. Lee, "Ge-photodetectors for Si-based optoelectronic integration," Sensors (Basel, Switzerland) **11**(1), 696–718 (2011).
19. L. Chen and M. Lipson, "Ultra-low capacitance and high speed germanium photodetectors on silicon," Optics Express **17**(10), 7901–7906 (2009).
20. M. Gould, T. Baehr-Jones, R. Ding, and M. Hochberg, "Bandwidth enhancement of waveguide-coupled photodetectors with inductive gain peaking," Optics Express **20**(7), 7101–7111 (2012).
21. R. Ding, T. Baehr-Jones, T. Pinguet, J. Li, N. C. Harris, M. Streshinsky, L. He, A. Novack, E.-J. Lim, T.-Y. Liow, H.-G. Teo, G.-Q. Lo, and M. Hochberg, "A Silicon Platform for High-Speed Photonics Systems," in *Optical Fiber Communication Conference*, OSA Technical Digest (Optical Society of America, 2012), paper OM2E.6.

1. Introduction

Silicon has in the past decade become the subject of intense interest for use in photonics. There are a number of advantages to using silicon as a platform for photonics including the high degree of confinement that silicon offers, the ability to leverage the fabrication knowledge and investments developed by the CMOS electronics industry and the possibility of integrating many components into complex photonic integrated circuits (PICs) [1]. Recently, the silicon photonics community has begun to move from working on individual devices to creating more complex systems [2]. However, continued effort into improving the performance of individual devices is required to ensure stability and raise the performance of such systems.

A critical component of the silicon photonics infrastructure is the germanium photodiode. Germanium is widely used as the detector absorption element due to its ability to absorb light at communications wavelengths and its CMOS compatibility. Techniques have been developed to grow germanium epitaxially on a silicon substrate with few defects [3-4]. However the relatively low absorption coefficient of germanium necessitates larger detectors to obtain reasonable responsivity. The increased area increases the capacitance of the detector junction, which correspondingly reduces the detector bandwidth. Significant work has been done to minimize this capacitance and develop high-speed waveguide-coupled germanium photodetectors [5-8]. By optimizing both the detector fabrication and geometry, detector bandwidth above 100 GHz has been reported [9]. However, for integrated photonics in silicon it is often not practical to optimize the process solely to lower detector capacitance.

Gain peaking is a technique that has been used in the design of electronics systems such as CMOS amplifiers [10-11] and photoreceiver amplification [12-14]. However, the authors are unaware of any previous demonstration of detector peaking that has been integrated directly on a silicon photonics chip. We have demonstrated that it is possible to significantly increase detector bandwidth using metal layers that are commonly available in CMOS-compatible silicon photonics processes [15].

2. Baseline Detector Modeling

Modeling of detectors can involve complex models and simulations [16-17]. Due to the small width of the intrinsic region of the germanium on silicon, waveguide-coupled detectors, the RC constant is the limiting factor in the bandwidth and transit time effects can be largely ignored [18-19]. The RC circuit often gives a reasonably accurate model for the response of a photodetector. We denote R_{load} as the load resistance, C_{pd} as the detector capacitance and R_{pd} as the detector resistance. The cutoff frequency for this simple model is given by Eq. 1.

$$f_c = \frac{1}{2\pi C_{pd}(R_{load} + R_{pd})} \tag{1}$$

We take the bandwidth denoted by f_c to be the 3dB point at which the photocurrent has been reduced by a factor of sqrt(2). The load resistance can be considered either the input to a transimpedance amplifier (TIA) or another type of 50-Ω load.

It is possible to increase the bandwidth by reducing either the detector capacitance or resistance. The detector capacitance scales with the area of the detector and is dependent on a number of variables such as the detector's intrinsic width and the doping concentrations. While the capacitance can be estimated analytically, it is more accurate to measure the capacitance for a given process. Using a number of test structures of different areas, the capacitance per unit area was measured as a function of voltage as seen in Fig. 1.

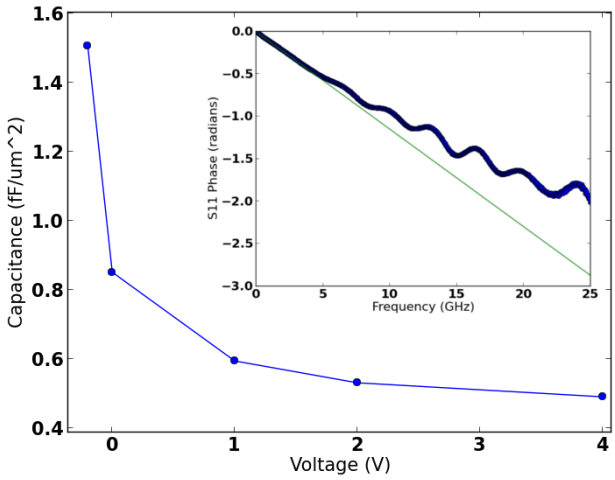

Fig 1. Junction capacitance per unit area as a function of reverse bias voltage (positive voltage on graph is reverse bias). The curve was measured by determining the capacitance from the detector S11 parameter (as seen in inset) using a number of test structures of different areas. The junction capacitance

In this work, the detectors were 8 um wide and 10 um long at the base with a 4x7.6 um junction for a junction capacitance of about 15 fF. As the detector area is minimized and the bias voltage increased, the capacitance of the photodetector is decreased and other parasitics in the circuit play a larger role. The largest of these parasitics is the capacitance due to the contact pads. The pads used in this study are 60 um x 60 um with a 100 um pitch and have a total capacitance of about 13 fF calculated by both simulation (Ansoft HFSS) and direct measurement. With smaller detectors, the parasitic pad capacitance is on the order of the detector capacitance and must be accounted for in the detector circuit model as a load parallel to the load resistance (C_{load}).

3. Gain Peaked Detector Modeling

It has previously been shown that adding an inductor to a photodetector circuit will act to increase the 3-dB bandwidth by peaking the EO response [20]. In order to evaluate how the detector circuit will respond to the addition of an inductor, we introduce another circuit model shown in Fig. 2.

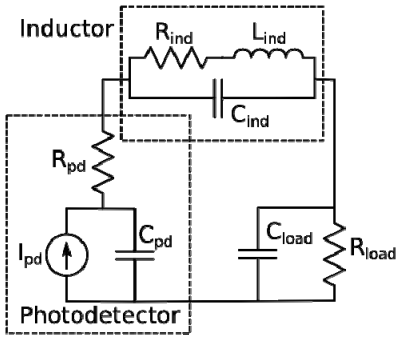

Fig 2. Gain peaking circuit model. The addition of an inductor is used to peak the frequency response of the photodetector.

In this model, a non-ideal inductor element [12-13] has been added that contains an inductance L_{ind} and a series resistance R_{ind} in parallel with a capacitance C_{ind}. The transfer function of this circuit is given by,

$$H(s)=\frac{V_{load}(s)}{I_{pd}(s)}=Z_{load}\cdot\left[R_{load}\cdot\left(C_{pd}\cdot s\cdot\left(R_{pd}+Z_{ind}+Z_{load}\right)\right)+1\right]^{-1} \tag{2}$$

$$s=j2\pi f \tag{3}$$

where the impedances Z_{ind} and Z_{load} are given by

$$Z_{ind}=1/(C_{pk}\cdot s+1/(L_{pk}\cdot s+R_{pk})) \tag{4}$$

$$Z_{load}=\frac{1}{C_{load}\cdot s+1/R_{load}} \tag{5}$$

Two different inductors were designed for use in gain peaking. Both inductors utilize two-loop square spiral geometries built using 1.5-um thick aluminum traces with 10-um width. The majority of the loop uses the thick top metal layer while only the metal crossing occurs in the thinner lower metal to minimize resistance. The small inductor (see Fig. 3) used an inner loop width of 20 um and an outer loop width of 50 um while the large inductor used a 50 um inner loop and an 80 um outer loop.

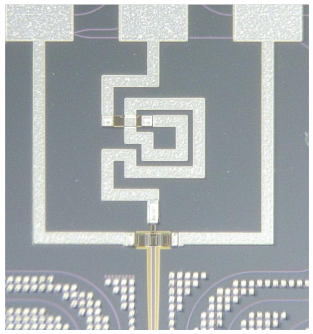

Fig. 3. Optical micrograph of the gain peaked photodetector using the 360 pH inductor. The inductor is approximately 100 um x 100 um in size.

Three-dimensional electromagnetic simulation was done on these inductor geometries using a commercial software package (Ansoft HFSS). The simulations showed that the small inductor had about 360 pH of inductance and 9.7 fF self-capacitance, while the large inductor had 580 pH of inductance and 19.8 fF self-capacitance. Both inductor elements had a relatively low series resistance of about $1\Omega/GHz^{1/2}$.

4. Fabrication

The detectors were fabricated at the Institute of Microelectronics (IME), a research institute of the Agency for Science, Technology and Research (A*STAR) as part of the OpSIS-IME MPW service [21]. The platform uses a 220 nm thick SOI wafer with 2-um buried oxide (BOX) as seen in Fig. 4. A 60 nm silicon etch is used to define the grating coupler layer while a 220 nm silicon etch is used to build the 500 nm waveguides.

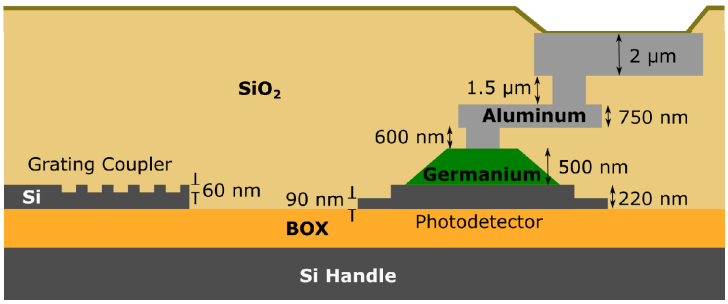

Fig 4. OpSIS-IME platform schematic. The detector is built using germanium grown epitaxially on unetched silicon. The inductors use the two metal layers. The lower via layer provides contact to the germanium. The anode of the detector is not shown.

The detector was built using selectively grown epitaxial germanium on top of the silicon. The germanium layer was 500 nm thick and had an angled sidewall. A 90 nm slab layer was also used to maximize the evanescent coupling between the silicon and the germanium. The silicon beneath the germanium was doped with boron to form the p-type side of the junction. The top of the germanium was implanted with phosphorous to form the n-type side of the p-i-n junction as seen in Fig. 5.

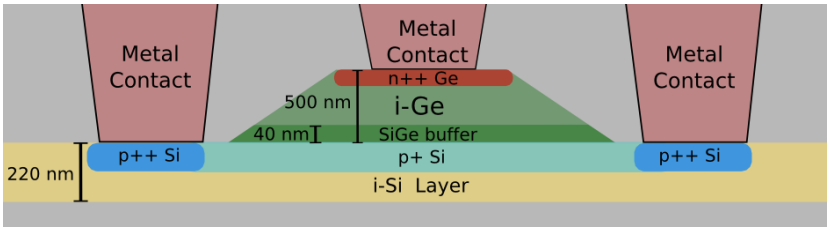

Fig 5. Photodetector cross section showing the detector p-i-n junction and metal contacts. The anode and cathode are shown.

A lower level of via was fabricated to contact both the n-type germanium as well as the p-type silicon. The first metal layer was then added, followed by an additional layer of vias and the second metal layer. An oxide cladding was deposited and opened above the metal pads that were used for probing the detector.

5. Experimental Results

5.1 Testing Configuration

The photodetectors were tested using a fiber array with polarization maintaining (PM) fiber to couple light on and off chip using a pair of grating couplers. A well-calibrated y-junction split the light path to go both to the detector and to an output grating coupler. This configuration allowed for accurate alignment to the grating couplers and precise calculation of the power incident on the detector.

For the detector S-parameter measurement, a vector network analyzer was used to drive a high-speed lithium niobate modulator and measure the detectors electrical response. The frequency response of the modulator was calibrated using an ultra-high-speed (70 GHz), commercial photodetector and normalized out of the response of the detector under test. A GSG microprobe was used to contact the metal pads of the detector.

5.2 Device Performance

Three detectors were tested to determine the efficacy of the gain peaking technique using the small inductor and the large inductor as well as a detector with no inductor to provide a baseline. Using a 2V reverse bias, DC responsivity and dark current were measured to be .75 A/W and 3 uA respectively with small variations between detectors due to fabrication-coupler alignment and fabrication variation. The approximate photodetector resistance (R_{pd}) was measured by fitting the IV curve of the detector at a forward bias of around 1V.

An EDFA was used to increase the signal to noise ratio and allow measurement of the detector response up to a frequency of 67 GHz as seen in Fig. 6. From the frequency response of these detectors, it is evident that gain peaking does have a significant effect at frequencies beginning around 10 GHz. The detector with no added inductance exhibits the lowest 3 dB bandwidth of around 30 GHz. The detector with the large, 580 pH inductor shows a large response peak near 35 GHz followed by a steep drop in response and a 3 dB bandwidth near 50 GHz. The detector with the small, 360 pH inductance on the other hand has less of an extreme peak, but has a higher 3 dB bandwidth near 60 GHz. A least-squares circuit model fit was obtained by using the simulated and measured detector parameters with the EO S21 response of Eq. 2. The fit parameters are shown in Table 1. A few of the fit values such as C_{pd} vary between detectors. This may be due to either fabrication variation of the p-i-n junction or an inexact fit of the detector response.

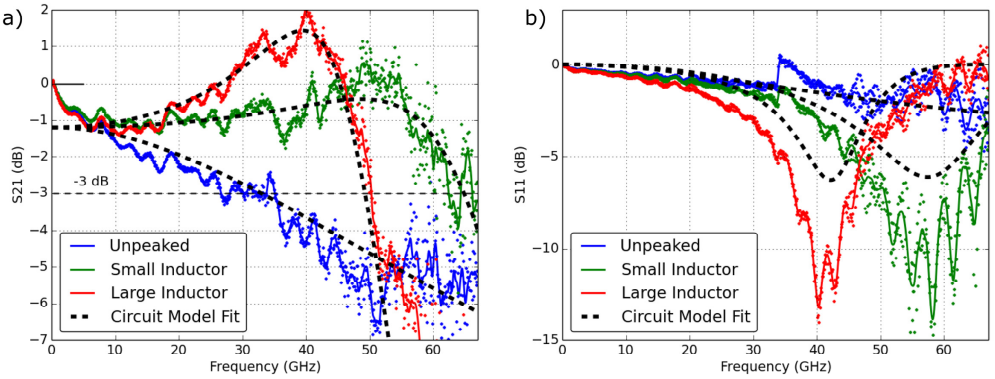

Fig 6. a) EO S21 and b) detector S11 response at 2V reverse bias of the unpeaked detector as well as the detectors with both small and large inductors. Points are from data, colored lines are smoothed data and black dashed lines are fits to the circuit model.

The above fits of EO S21 are fairly accurate in both the frequency of the peaking and magnitude of the peaking. However, there is a small discrepancy in the EO S21 fit at lower frequencies that is likely due to measurement error.

Table 1. Fit and expected photodetector parameters. For values that vary between the detectors, three measurements are shown for the unpeaked/small inductance/large inductance detectors.

Parameter	Fit Value	Expected Value
R_{pd}	140 Ohms	125 Ohms[m]
C_{load}	13 fF	13 fF[m]
C_{pd}	17/14/15 fF	15 fF[m]
L_{ind}	0/360/580 pH	0/360/580 pH[s]
C_{ind}	1/8/10 fF	0/9/20 fF[s]
R_{ind}	0 Ohms	1.2 Ohms/GHz$^{1/2}$ [s]

[m]Parameter measured directly from photodetectors

[s]Parameter found via simulation

The phase delay is calculated from the model and closely fits the measured phase as seen in Fig. 7a. The addition of an inductor increases the group delay variation as seen in Fig. 7b from -1.5 ps at 40 GHz for the unpeaked detector to 2.1 ps and 12.3 ps at 40 GHz for the small inductor and large inductor respectively. The group delay of the large inductor detector is approaching the 25 ps period at 40 GHz, which may negatively impact digital signal quality. We do not expect a significant increase in detector noise from the inductor as shown in [20].

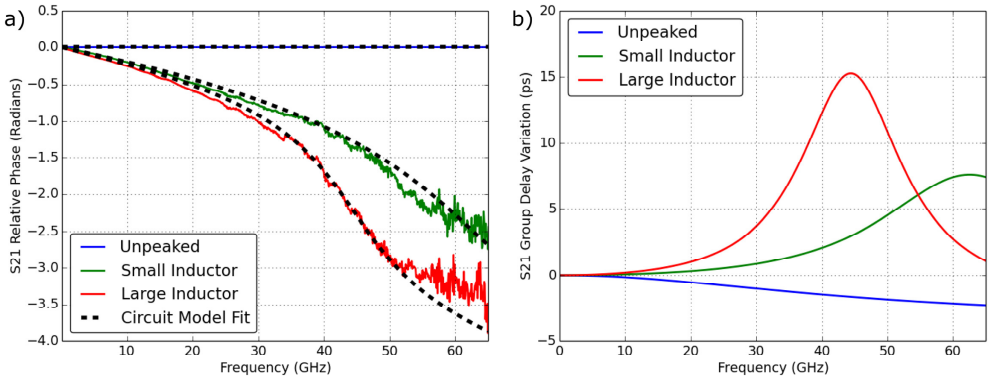

Fig 7. a) Phase delay of EO S21 normalized to the unpeaked detector. b) Group delay variation of EO S21 calculated from the circuit model fit to show effective group delay variation of measured data.

6. Conclusion

We have shown experimental evidence that the bandwidth of germanium on silicon can be significantly enhanced with the addition of a peaking inductor. The inductor can be fabricated with metal processes that currently exist on CMOS-compatible integrated photonics platforms. Using a spiral inductor of 360 pH, the bandwidth of a non-peaked detector was enhanced from 30 GHz to 60 GHz.

Acknowledgments

The authors would like to thank Gernot Pomrenke, of the Air Force Office of Scientific Research, for his support under the OPSIS (FA9550-10-1-0439), PECASE (FA9550-10-1-0053) and STTR (FA9550-12-C-0079) programs, and would like to thank Mario Paniccia and Justin Rattner, of Intel, for their support of the OpSIS program. Additionally, the authors are grateful for support from an MOE ACRF Tier-1 NUS startup grant.